

Atmosphere controlled conductivity and Maxwell-Wagner relaxation in $\text{Bi}_{0.5}\text{K}_{0.5}\text{TiO}_3 - \text{BiFeO}_3$ ceramics

M. I. Morozov, M. - A. Einarsrud, and T. Grande,

Department of Materials Science and Engineering, Norwegian University of Science and Technology, NO-7491 Trondheim, Norway

Here, we report on a giant dielectric relaxation in $(1-x)\text{Bi}_{0.5}\text{K}_{0.5}\text{TiO}_3 - x\text{BiFeO}_3$ ceramics below ~ 300 °C, which becomes more pronounced with increasing BiFeO_3 content. The relaxation was shown to be of Maxwell-Wagner type and associated with charge depletion at the electroded interfaces. It was also shown that the relaxation could be controlled or, eventually, could be removed by heat treatment in controlled partial pressure of oxygen. This was rationalized by the relationship between the electrical conductivity and variation in the oxidation state of Fe, which is strongly coupled to the partial pressure of oxygen. The results are discussed with emphasis on oxygen diffusion and point defect equilibria involving oxygen vacancies and iron in divalent and tetravalent state. Finally, the barrier-free dielectric properties of the $(1-x)\text{Bi}_{0.5}\text{K}_{0.5}\text{TiO}_3 - x\text{BiFeO}_3$ ceramics are reported.

I. INTRODUCTION

Solid solutions of $(1-x)\text{Bi}_{0.5}\text{K}_{0.5}\text{TiO}_3 - x\text{BiFeO}_3$ (BKT – BFO, or BKTF- x (%)) have attracted recent attention¹⁻⁹ owing to their promising electromechanical properties^{1,6} reaching maximum values both with respect to electrostriction⁷ and piezoelectricity⁹ and relation to multiferroicity⁸.

Bismuth ferrite has all prerequisites for high-temperature piezoelectric application, including high spontaneous polarization ($\sim 90 \mu\text{C}/\text{cm}^2$) and strain,^{10,11} as well as high Curie temperature ($T_C \sim 820 \text{ }^\circ\text{C}$).^{10,12} However, practical exploration of these advantages usually meets challenges with fabrication of BFO into dense and single-phase ceramics by conventional solid state processing, high electrical conductivity, and finally high coercive fields, possibly enhanced by domain wall pinning effects.^{10,13-15} These challenges result in unstable or weakly reproducible piezoelectric performance of BFO ceramics.^{10,14,15} Furthermore, the rise of ac conductivity at low frequencies or at high temperatures results in colossal dielectric response due to Maxwell-Wagner (MW) relaxation.^{10,16-19} The MW relaxation may originate from the inherent impurity of BFO ceramics, but can possibly be explained by a charge-depleted interface layer at the surface, as reported for BFO single crystals.¹⁹

The BFO-rich compositions with $x \geq 0.7$ in the BKT-BFO system are isostructural to ferroelectric BFO ($R3c$)^{1,3,7,9} and thus can be considered as alternatives to pure bismuth ferrite. Compositional modification of BFO with BKT leads to higher thermodynamic stability of the perovskite phase and results in dense and phase pure ceramics.^{1,3,6-8} The BKTF ceramics with $x \geq 70\%$ still possess relatively high T_C (above $450 \text{ }^\circ\text{C}$),⁸ show significantly better stability of electric field induced strain, and slightly lower coercive field.⁹

The electrical conductivity of BFO was reported to be of *p*-type,²⁰⁻²¹ and lately suggested to be controlled by the oxidation state of Fe.^{22,23} Similar conductivity mechanism is therefore anticipated in BFO-rich BKTF ceramics.⁹

In this study we report on the permittivity and electrical conductivity of BKT-BFO ceramics during thermal cycling in various atmospheres. We demonstrate how MW relaxation in BKT-BFO ceramics can be controlled by the partial pressure of oxygen, reflecting the importance of point defect chemistry coupled to oxidation/reduction of Fe at the surface and in the bulk of the ceramics. Finally, we address the barrier-free dielectric response in a wide range of BKT-BFO compositions.

II. EXPERIMENTAL

Samples of $(1-x)\text{Bi}_{0.5}\text{K}_{0.5}\text{TiO}_3 - x\text{BiFeO}_3$ ceramics in the composition range $0.1 \leq x \leq 0.9$ were prepared by the conventional solid state reaction method as described previously.^{6,7} The materials were all phase pure and dense ($\sim 98\%$ density) and with relatively fine grains ($\sim 0.5 - 3 \mu\text{m}$). The phase purity of the materials was confirmed by X-ray diffraction analysis and scanning electron microscopy. The surfaces of sintered ceramic pellets were grinded, polished, carefully cleaned using ultrasound bath, and electroded with sputtered gold or painted silver. The final thickness of the samples ranged within 1 - 4 mm.

The dielectric spectroscopy was performed using an Alpha-A impedance analyzer (Novocontrol, Germany) in two regimes: 1) at normal ambient conditions, using a Novotherm (Novocontrol, Germany) testing chamber allowing precise temperature control ($\pm 0.5 \text{ }^\circ\text{C}$), stepwise or with continuous temperature ramping of $2 \text{ }^\circ\text{C}/\text{min}$; 2) in a Probostat (Norecs, Norway) testing chamber. The chamber was flushed with a sweep gas of either dry synthetic air,

pure O₂, or Ar/H₂ (95/5) gas mixture at a low flow rate. The impedance measurements were performed every 30 seconds during heating and cooling with approximate ramping of 2 °C/min. Impedance data were processed using WinFIT (Novocontrol, Germany) software.

In order to distinguish between the dielectric permittivity of bulk BKTF ceramics and the value directly derived from the experimentally measured capacitance of samples under test, we use the following definition:

$$\tilde{\epsilon}'_r = \frac{C'h}{\epsilon_0 A},$$

where C' is the real part of the measured capacitance of electroded BKTF samples, h is the sample thickness, A is the area of electroded surface, and ϵ_0 is the dielectric permittivity of vacuum.

Some of the electroded samples were subjected to thermogravimetric analysis up to 700 °C, using a STA 449 C Jupiter thermal analyzer coupled with a QMS 403C Aëolos mass spectrometer (Netzsch, Germany).

III. RESULTS AND DISCUSSION

A. Origin of Maxwell-Wagner relaxation

The temperature dependent dielectric response across the composition of (1-x)BKT – xBFO is shown in Fig. 1 (a)-(d). A rise of a dielectric peak $\tilde{\epsilon}'_r(T)$ at low frequencies was

observed with increasing BFO content. At low BFO content the maximum is hardly observable, while at high BFO content a broad maximum is strongly pronounced.

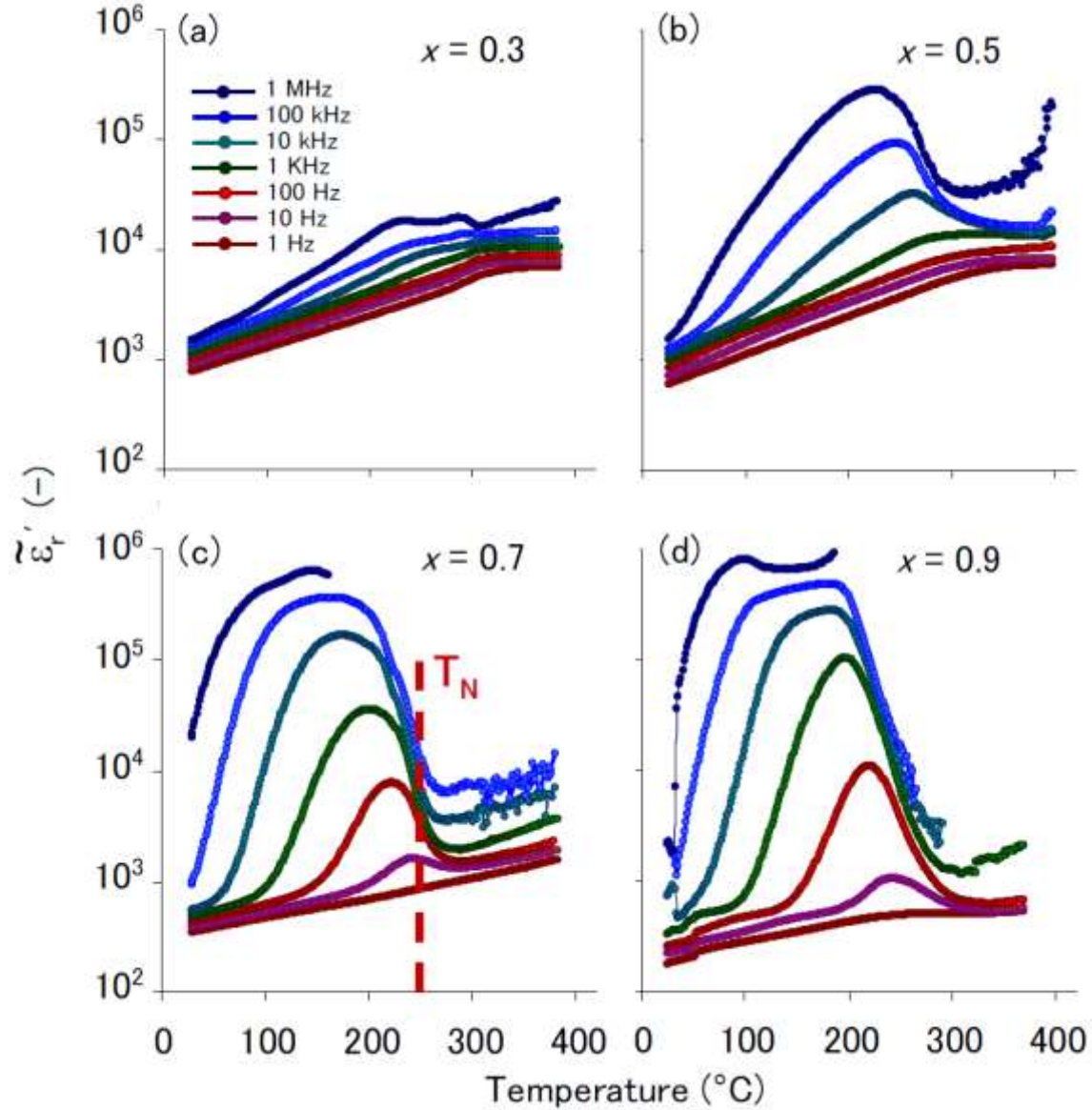


FIG. 1. (Color online) Dielectric response of $(1-x)\text{BKT} - x\text{BFO}$ ceramics with Au electrodes measured upon heating in air: (a) $x = 0.3$; (b) $x = 0.5$; (c) $x = 0.7$; (d) $x = 0.9$. The Neel temperature for BKTF-70 is taken from Ref.⁸

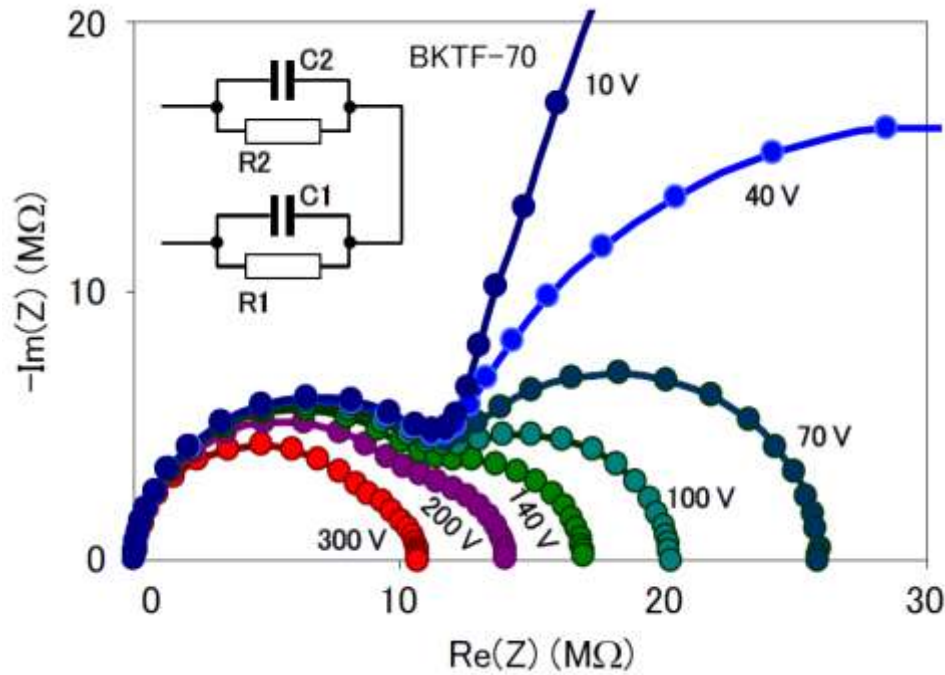


FIG. 2. (Color online) Impedance complex plane plot for BKTF-70 ceramics as a function of ac voltage amplitude (rms). Inset: the equivalent circuit used for modeling the impedance data.

Considering the giant magnitude of the observed dielectric peaks, they are interpreted as a signature of MW relaxation²⁴⁻²⁷ rather than manifestation of a ferroelectric relaxor response,²⁶ also known for BKTF compositions with $x < 0.7$.¹⁻⁷ In order to ascertain this, impedance spectroscopy was performed at room temperature with various amplitudes of the driving ac voltage. The result is shown in Fig. 2 for BKTF-70. The observed impedance fits classic response of a MW system with equivalent circuit consisting of two lossy dielectric components in series: the bulk (R_1, C_1) and barrier (R_2, C_2), as shown in the inset of Fig. 2. The voltage dependent barrier relaxation is a clear indication of its interfacial origin with local charge depletion, such as a Schottky barrier.²⁷ Analysis of Schottky barriers in ferroelectrics is not trivial and may require

consideration of the polarization reversal effects^{28,29} as well as conductive domain walls,³⁰ but possible contributions from these effects is not pursued any further in this study.

In order to estimate evolution of the bulk and barrier contributions with increasing temperature, impedance spectroscopy was performed on a BKTF-60 sample at stepwise increasing temperature. The parameters of the equivalent circuit model (Fig. 2) are shown as functions of temperature in Fig. 3 (a). An estimation of the barrier thickness and concentration of mobile charge carriers was performed as follows. Let us first expand the resistances and capacitances for the bulk and barrier contributions with indices $i = 1$ and $i = 2$, respectively, according to the following:

$$R_i = \rho_i \frac{h_i}{A} = \frac{h_i}{Aqn_i\mu_i}, \quad C_i = \varepsilon_0\varepsilon_r^{(i)} \frac{A}{h_i}$$

where h is thickness, ε_r is the relative dielectric permittivity, ρ is the resistivity; n is the concentration of major charge carriers, μ is their mobility in the corresponding layers, q is the elementary electric charge, ε_0 is the dielectric permittivity of vacuum, and A is the sample area. Assuming that the dominating charge carriers are polarons hopping between localized states associated with Fe^{4+} ,^{22,23} i.e. $n_i \approx [Fe_{Fe}^{\bullet}]_i$, and that the mobility and the relative dielectric permittivity are equal in the bulk and in the barrier, $\mu_1 \approx \mu_2$ and $\varepsilon_r^{(1)} \approx \varepsilon_r^{(2)}$, the following relationships between the thickness and free charge carrier concentrations can be derived:

$$\frac{h_2}{h_1} = \frac{C_1}{C_2} \quad \text{and} \quad \frac{[Fe_{Fe}^{\bullet}]_2}{[Fe_{Fe}^{\bullet}]_1} = \frac{R_1C_1}{R_2C_2}$$

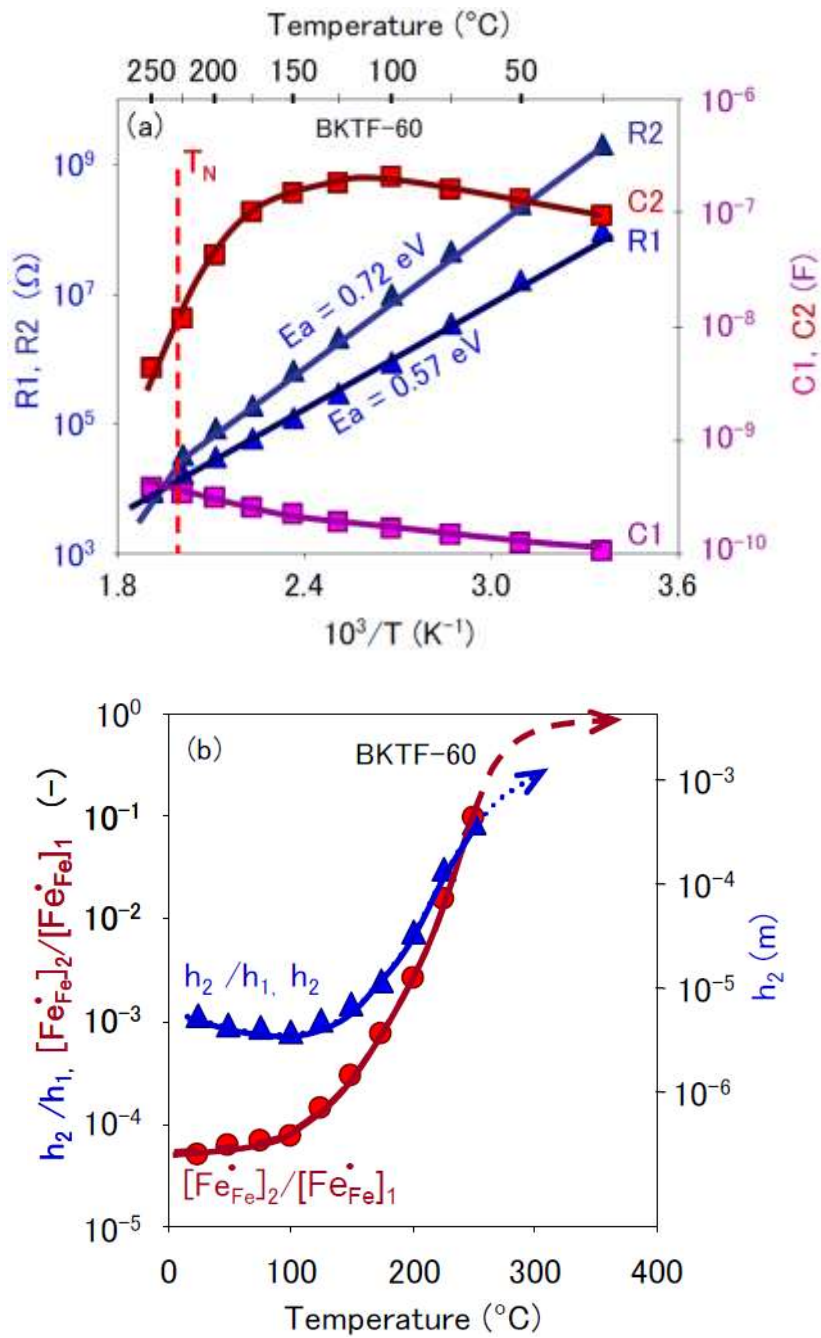
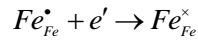


FIG. 3. (Color online) (a) Temperature dependence of the modeling equivalent circuit parameters for impedance of BKTF-60 ceramics. The Neel temperature T_N is indicated⁸. (b) Corresponding depletion layer thickness h_2 and the barrier/bulk ratios for h_2/h_1 and $[Fe_{Fe}^{\bullet}]_2/[Fe_{Fe}^{\bullet}]_1$ as a function of temperature.

These dependencies are shown in Fig. 3 (b) as a function of stepwise rising temperature. At room temperature the concentration of mobile charge carriers in the depletion layer is approximately four orders of magnitude lower than in the bulk, while the thickness of the depletion layer is approximately 3 orders of magnitude lower. For the given sample thickness (~ 4.5 mm) the width of the depletion layer is estimated to be ~ 5 μm . For comparison, the width of potential barrier interface in ferroelectric lead zirconate titanate films ranges within 3 – 30 nm.²⁹ Thus, in spite of the observed manifestation of electronic barrier properties, the contributing charge-depleted layer cannot be entirely rationalized by the Schottky barrier formation. Seemingly, some other mechanisms may contribute. In support of this consideration, BFO single crystals are known to develop an inherent “skin layer” with electronically different properties at the surface, which can be probed without any metallic contact.¹⁹

We propose that the depletion layer is a region with reduced concentration of 4-valent iron point defects Fe_{Fe}^{\bullet} , the main charge carrier assuming p -type conductivity.^{22,23} Then the formation of a depletion layer at a Schottky interface can be expressed as an electron transfer from the metal electrode:



Annihilation of the barrier due to increase of the Fe_{Fe}^{\bullet} concentration in the depleted region upon heating can be rationalized by the point defect equilibrium involving oxidation of Fe^{3+} (Fe_{Fe}^{\times}) taking place at the surface:



Thus, the temperature evolution shown in Fig. 3 (b) can be rationalized assuming two plausible processes: (1) oxidation at the surface and (2) diffusion of oxygen vacancies from the interior of the sample. Both processes lead to "dilution" of the depleted layer into the bulk. The annihilation condition for the depleted layer is either $h_2 / h_1 \rightarrow \infty$ or $[Fe_{Fe}^{\bullet}]_2 / [Fe_{Fe}^{\bullet}]_1 \rightarrow 1$. Considering the large increase in $[Fe_{Fe}^{\bullet}]_2 / [Fe_{Fe}^{\bullet}]_1$, the latter condition is expected to be fulfilled first at temperatures above 250 °C (Fig. 3(b)). Thus the depletion layer vanishes at temperatures ~ 300 °C reaching approximately 10% of the sample thickness (~ 50 μm). The change in the thickness of the depletion layer is most likely dominated by diffusion of oxygen ions from the surface into the bulk. The diffusion constant of the process can be roughly estimated as $D_o = 4L^2 / t$, where $L \approx 5$ μm (thickness of the depletion layer) and $t \approx 120$ s (timescale of a 10 degrees interval), which gives $D_o \sim 8 \cdot 10^{-8}$ cm^2s^{-1} . This is $10^1 - 10^2$ higher than the self-diffusion coefficient of oxygen vacancies (D_v) in LaFeO_3 ,³¹ a material isostructural to paraelectric BFO.³² We find this reasonable taking into account that this is a chemically driven diffusion and that the oxygen diffusion coefficient is proportional to the concentration of oxygen vacancies ($D_o = C_v / C_o \cdot D_v$, where C_v / C_o is the relative concentration of vacancies at the oxygen sub-lattice) originated from the loss of Bi_2O_3 during processing.

Fig. 4 illustrates the evolution of ac conductivity $\sigma'(T)$ measured in BKTF-70 ceramics upon heating with a constant rate of 2 °C/min. Depending on frequency and temperature, the real part of the ac conductivity is dominated by either bulk or barrier contributions, each of which is dominated either by its dc component ($\sigma_{dc}(\text{bulk})$, $\sigma_{dc}(\text{barrier})$) – at lower frequencies, or by its “dielectric loss” component ($\omega\varepsilon_0\varepsilon''(\text{bulk})$, $\omega\varepsilon_0\varepsilon''(\text{barrier})$) – at higher frequencies. Due to the

thermal activation of the dc components, they are straight lines in an Arrhenius plot, while the frequency dependent “loss” contributions are weak functions of temperature and show “stairs” of higher-frequency “plateaus”. Thus, the bulk and barrier contributions can also be clearly distinguished in Fig. 4.

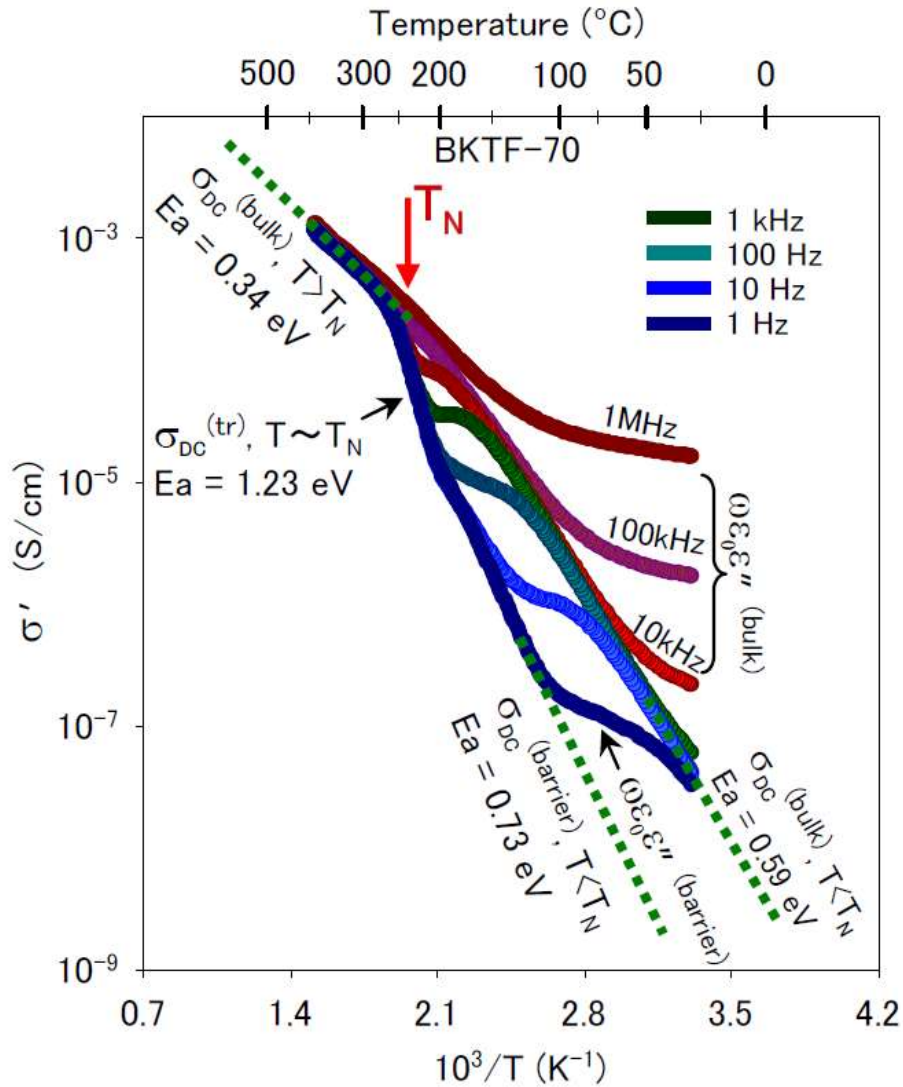


FIG. 4. (Color online) Real part of complex conductivity as a function of temperature measured in untreated BKTF-70 ceramics during heating. The Neel temperature is shown according to Ref.⁸

The activation energies for the bulk and barrier conductivities in BKTF-70 ceramics are 0.59 and 0.72 eV, nearly the same as we determined for BKTF-60 ceramics by analyzing the temperature dependence of the equivalent circuit resistances R1 and R2 shown in Fig. 3 (a).

The process of barrier annihilation under dynamic condition is shown in Fig. 4, in contrast to the stepwise heating experiment illustrated in Fig. 3. A rapid increase of barrier conductance at the narrow temperature range (200 – 280 °C) with activation energy $E_a = 1.23$ eV suggests a very rapid increase of the concentration of mobile charge carriers in the depletion region. The same experiment performed within a complete heating-cooling cycle in dry synthetic air showed irreversible annihilation of the interface barrier: no manifestation of MW relaxation was observed upon cooling (e.g. Fig. 5 (a)) and at room temperature. This is another indication that the oxidation reaction (1) occurs during heat treatment in synthetic air.

B. Control of bulk and barrier conductivity

In this section we address the possibility to control conductivity both at the surface and further into the bulk by the point defect reactions influencing the oxidation state of Fe and thereby the concentration of the major charge carriers.

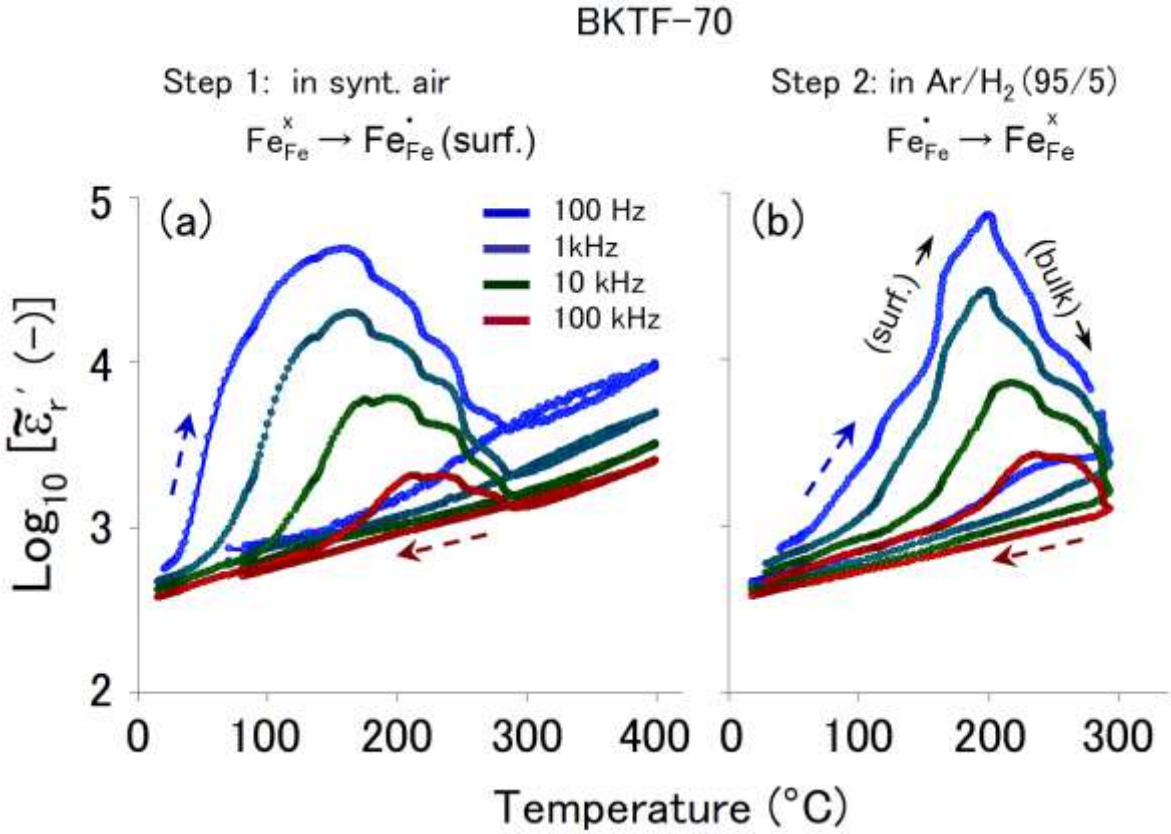


FIG. 5. (Color online) Dielectric response of BKTF-70 ceramics measured in two heating-cooling sequences: (a) in dry synthetic air and (b) in Ar/H₂ (95/5) gas mixture. Arrows indicate heating and cooling paths.

The dielectric responses measured in a sequence of heating-cooling cycles in various atmospheres are shown in Fig. 5. At the first cycle performed in dry synthetic air, the observed MW relaxation appeared only upon heating and did not manifest itself upon cooling (Fig. 5 (a)). This suggests annihilation of the charge-depleted layer through the oxidation reaction (1), as discussed in the previous section. The second heating-cooling cycle was performed in Ar/H₂ (95/5) gas mixture. The MW relaxation peaks reappeared in the dielectric response upon heating

and, again, disappeared upon cooling, as shown in Fig. 5 (b). The conductive response throughout this cycle is also indicated by curve (1) in Fig. 6. Comparison of the dielectric response and conductivity changes due to thermal treatment in the reducing atmosphere suggests formation of charge-depleted layer at the surface below 200 °C (surface reaction) with further propagation into the bulk at temperatures 200 – 290 °C (bulk diffusion). The initial point defect equilibrium in reducing atmosphere is opposite to (1):



Thus, reaction (2) reduces the concentration of the major charge carriers and leads to charge depletion. This rationalizes the observed impedance behavior as follows. Formation of a charge depleted layer, first, at the surface results in MW relaxation and strong frequency dispersion of dielectric response reaching the peak value at ~200 °C (Fig. 5 (b)). Farther diffusion of oxygen vacancies into the bulk at higher temperatures homogenizes the distribution of point defects thus reducing, first, the MW relaxation (Fig. 5(b)), then the bulk conductivity (Fig. 6).

In case of heating above 290 °C in the reducing Ar/H₂ (95/5) atmosphere (curve (2) in Fig. 6), the bulk conductivity showed a rapid increase. This suggests the change and further domination of *n*-type conductivity associated with divalent iron point defects (Fe'_{Fe}):



Thus, heat treatment of BKTF-70 ceramics in reducing atmosphere is shown to shift the original *p*-type conductivity towards *n*-type through the dynamically established minimum at ~290 °C with the heating rate of 2 °C/min used in our experiments. It is, therefore, reasonable to assume

that the static equilibrium could be achieved at slightly lower temperature. When the dynamic heating experiment was interrupted at ~ 290 °C, as in the case of sample (1) in Fig. 6, the conductivity upon cooling remained reduced down to room temperature. Thus, this manipulation also resulted in lower bulk conductivity at room temperature.

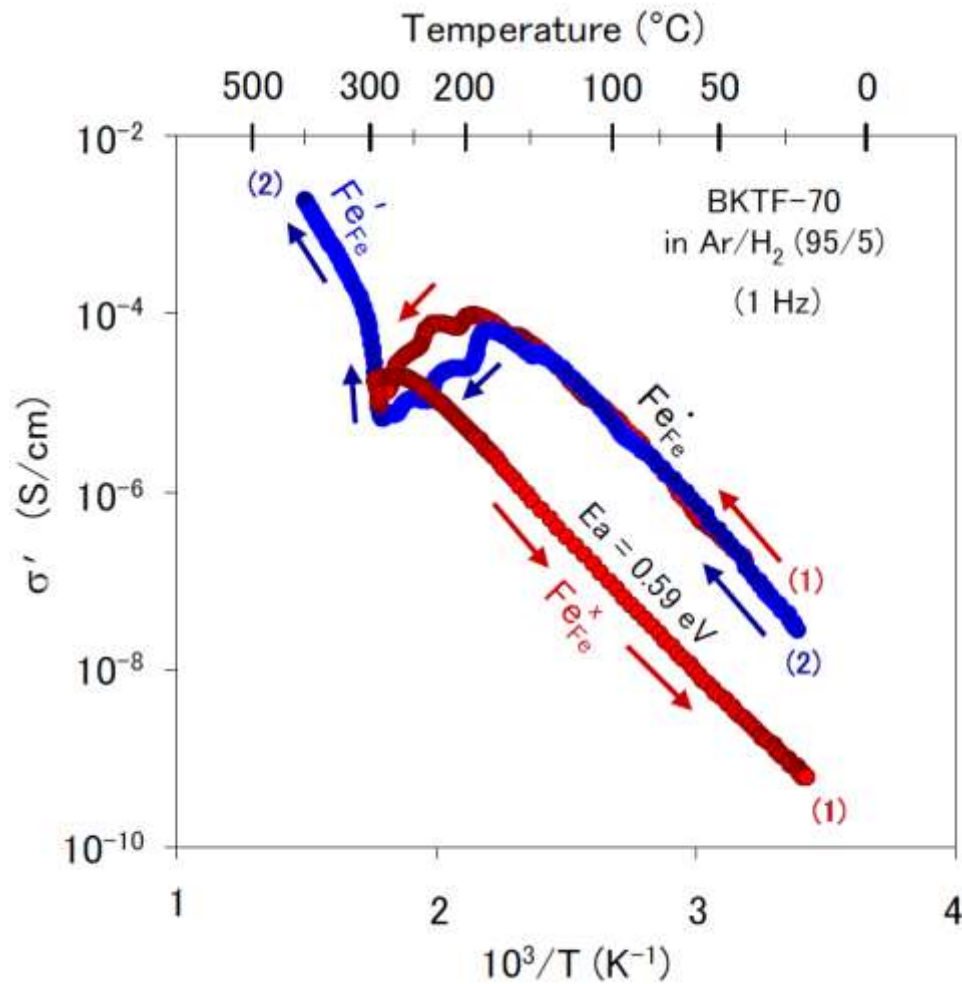


FIG. 6. (Color online) Real part of the complex conductivity (1 Hz) for BKTF-70 ceramics upon thermal cycling in Ar/H₂ (95/5) gas mixture. Numbers in brackets and arrows designate different samples and their thermal paths (see comments in the text).

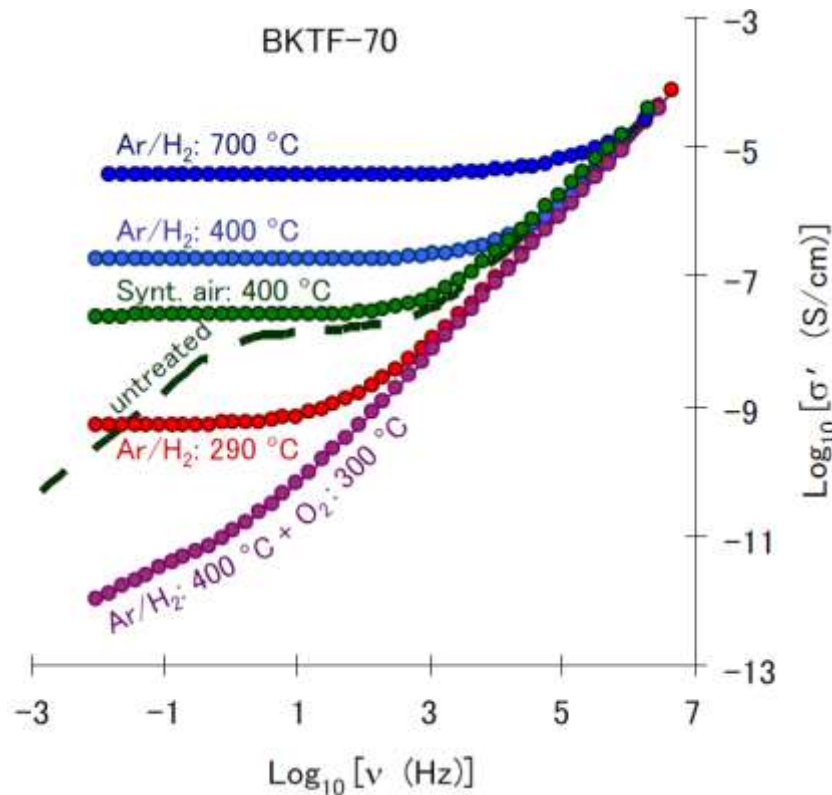


FIG. 7. (Color online) Room temperature dispersion of the real part of ac conductivity in BKTF-70 ceramics treated in various atmospheres.

Fig. 7 summarizes the effects of thermal treatment in reducing and oxidizing atmospheres on the ambient bulk conductivity of BKTF-70. The dashed line indicates the ac conductivity of the untreated sample, showing classical MW relaxation with tendency to form the second dc-plateau at frequencies below 1 mHz, where the resistive impedance of the depletion layer will dominate the reactive part. Thermal annealing in air at 400 °C removed the barrier without affecting the bulk conductivity. Other redox reactions performed in Ar/H₂ and O₂ are shown to

affect the bulk conductivity without forming of the charge-depleted layer at the surface. This indicates that propagation of these reactions into the bulk becomes significant already at temperatures as low as 300 °C. This also implies sufficient mobility of oxygen vacancies at these temperatures.

We also considered possible influence of hydrated oxygen vacancies to the permittivity, but in situ thermogravimetric analysis combined with mass spectroscopy did not give any evidence of water adsorbed at the surface or dissolved in the bulk.

C. Barrier-free properties

The elimination of interface barrier by thermal treatment in dry air allowed us to distinguish between Maxwell-Wagner relaxation related to charged-depleted interface and the true relaxor behavior in the BKT-BFO system. The barrier-free dielectric response as a function of temperature and frequency for various BKTF compositions is shown in Fig. 8 (a)-(e). Relaxor-like dielectric responses were observed for compositions with $x < 0.7$, while a ferroelectric-like sharp dielectric peak was observed in BKTF-70 ceramics and thus also anticipated for compositions with higher BFO content. This is in good agreement with careful microstructure analysis previously reported for this system.³

Overall, the temperature dependent dielectric response showed a smooth transformation across the BKT – BFO system (Fig. 8 (f)): as BFO content increases the dielectric peak in pseudocubic phase ($x < 0.7$) becomes sharper, steadily approaching the shape of the peak in ferroelectric phase ($x \geq 0.7$).

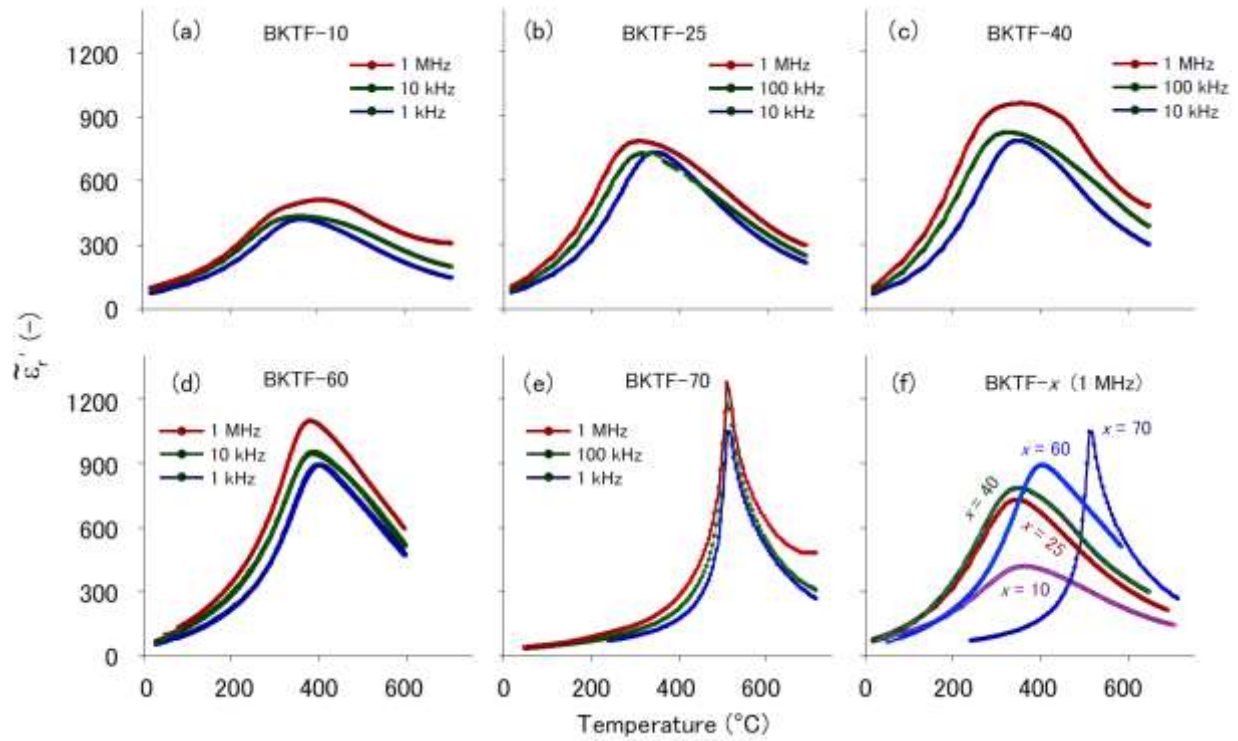


FIG. 8 (Color online) Relative dielectric permittivity as a function of temperature and frequency for BKTF- x (%) ceramics: (a) $x = 10$; (b) $x = 25$; (c) $x = 40$; (d) $x = 60$; (e) $x = 70$; (f) $x = 10 - 70$, at 1 MHz.

D. Anomalies around Neel temperature

It is noteworthy that the key temperature region around ~ 290 °C, where the MW relaxation disappears irrespectively of redox reactions coincides with Neel temperatures reported for some of BKTF compositions⁸ (e.g. Neel temperature is shown in Fig. 1 (c), 3 (a), and 4). Another evidence of the vicinity of Neel temperature at the region where MW relaxation annihilates is the slope deflection of bulk conductivity $\sigma_{DC}^{(bulk)}(T)$ in Arrhenius scales, as shown in Fig. 4. The latter anomaly is likely a characteristic feature of the antiferromagnetic –

paramagnetic phase transition, also observed in other antiferromagnets including BiFeO₃ at T_N ~ 370 K^{10,13} and BiMnO₃ at T_N ~ 100 K.^{33,34}

In spite of the likely accidental coincidence of Neel point with the redox reactions temperature, it is possible that the MW relaxation (observed in this study only in antiferromagnetic state) is enhanced by a magnetoresistive phenomenon, as predicted and observed in other materials with magnetic order.³⁵⁻³⁷ Our study does not provide any experimental support to this consideration, except an apparent correlation between the increasing magnitude of MW dielectric dispersion and concentration of antiferroelectric BFO component in the system (Fig.1).

IV. CONCLUSION

The dielectric properties and conductivity of BKT-BFO ceramics were examined during heating and cooling in various atmospheres with controlled oxygen partial pressure. It was demonstrated that the conductivity and MW relaxation in these ceramics can be controlled by oxygen partial pressure during thermal treatment at relatively low temperatures. The observed variation of conductivity is rationalized by point defect reactions describing interplays between oxygen vacancies and the oxidation state of iron. The suggested mechanisms and processes can be anticipated in pure BFO and related materials with *p*-type conductivity associated with 4-valent iron point defects.^{22,23}

ACKNOWLEDGMENT

The work was carried out within the LEADFREE research project financed by the Norwegian Research Council, FRINATEK grant 197497.

References

- ¹H. Matsuo, Y. Noguchi, M. Miyayama, M. Suzuki, A. Watanabe, S. Sasabe, T. Ozaki, S. Mori, S. Torii, and T. Kamiyama, *J. Appl. Phys.* **108**, 104103 (2010).
- ²J.M. Kim, Y.S. Sung, J.H. Cho, T.K. Song, M.H. Kim, H.H. Chong, T.G. Park, D. Do, and S.S. Kim, *Ferroelectrics* **404**, 88 (2010).
- ³T. Ozaki, H. Matsuo, Y. Noguchi, M. Miyayama, and S. Mori, *Jap. J. Appl. Phys.* **49**, 09MCO5 (2010).
- ⁴A.V. Pushkarev, N.M. Olekhovich, and Yu.V. Radyush, *Inorg. Mater.* **47** [7] 774 (2011).
- ⁵A.V. Pushkarev, N.M. Olekhovich, and Yu.V. Radyush, *Phys. Solid State* **53** [3] 522 (2011).
- ⁶M.I. Morozov, M.-A. Einarsrud, T. Grande, and D.Damjanovic, *Ferroelectrics* **439**, 88 (2012).
- ⁷M.I. Morozov, M.-A. Einarsrud, and T. Grande, *Appl. Phys. Lett.* **101**, 252904 (2012).
- ⁸J. Bennett, A.J. Bell, T.J. Stevenson, R.I. Smith, I. Sterianou, I.M. Reaney, and T.P. Comyn, *Mater. Lett.* **94**, 172 (2013)
- ⁹M.I. Morozov, T. Grande, and M.-A. Einarsrud, "Control of conductivity and piezoelectric performance in bulk $\text{Bi}_{0.5}\text{K}_{0.5}\text{TiO}_3 - \text{BiFeO}_3$ Ceramics, *in preparation*.
- ¹⁰G. Catalan and J.F. Scott, *Adv. Mater.*, **21**, 2463 (2010).
- ¹¹P.Ravindran, R. Vidya, A. Kjekshus, and H. Fjellvåg, *Phys. Rev. B* **74**, 224412 (2006).
- ¹²S.A. Fedulov, *Dokl. Akad. Nauk SSSR* **139**, 1345 (1961); [English Transl.: *Sov. Phys. Dokl.* **6**, 729 (1962)].
- ¹³S.M. Selbach, M.-A. Einarsrud, and T. Grande, *Chem. Mater.* **21**, 169 (2009).

- ¹⁴T. Rojac, M. Kosec, B. Budic, N. Setter, and D. Damjanovic, *J. Appl. Phys.*, **108**, 074107 (2010).
- ¹⁵T. Rojac, M. Kosec, and D. Damjanovic, *J. Am. Ceram. Soc.* **94** [12], 4108 (2011).
- ¹⁶R. Mazumder, S. Ghosh, P. Mondal, D. Bhattacharya, S. Dasgupta, N. Das, A. Sen, A.K. Tyagi, M. Sivakumar, T. Takami, H. Ikuta, *J. Appl. Phys.* **100**, 033908 (2006).
- ¹⁷S. Kamba, D. Nuzhnyy, M. Savinov, J. Šebek, J. Petzelt, J. Prokleška, R. Haumont, J. Kreisel, *Phys. Rev. B* **75**, 024403 (2007).
- ¹⁸P. Tirupathi and A. Chandra, *J. Alloys and Compounds* **564**, 151 (2013).
- ¹⁹X. Marti, P. Ferrer, J. Herrero-Albillos, J. Narvaez, V. Holy, N. Barrett, M. Alexe, and G. Catalan, *Phys. Rev. Lett.* **106**, 236101 (2011).
- ²⁰Z. Zhang, P. Wu, L. Chen, and J. Wang, *Appl. Phys. Lett.* **96**, 232906 (2010).
- ²¹T.R. Paudel, S.S. Jaswal, and E.Y. Tsybal, *Phys. Rev. B* **85**, 104409 (2012).
- ²²N. Maso and A.R. West, *Chem. Matter.* **24**, 2127 (2012).
- ²³A.R. Makhdoom, M.J. Akhtar, R.T.A. Khan, M.A. Rafiq, M.M. Hasan, F. Sher, and A.N. Fitch, *Mater. Chem. Phys.* **143**, 256 (2013).
- ²⁴P. Lunkenheimer, V. Bobnar, A.V. Pronin, A.I. Ritus, A.A. Volkov, and A. Loidl, *Phys. Rev. B* **66**, 052105 (2002).
- ²⁵P. Lunkenheimer, S. Krohus, S. Riegg, S.G. Ebbinghaus, A. Reller, and A. Loidl, *Eur. Phys. J. Special topics* **180**, 61 (2010).
- ²⁶A.A. Bokov and Z.-G. Ye, *J. Adv. Dielect.* **2**, 1241010 (2012).
- ²⁷S.M. Sze, *Semiconductor Devices: Physics and Technology*, 2nd Ed. (Wiley, New York, 2001)
- ²⁸L. Pintilie and M. Alexe, *J. Appl. Phys.* **98**, 124103 (2005).
- ²⁹L. Pintilie, I. Boerasu, M.J.M Gomes, T. Zhao, R. Ramesh, and M. Alexe, *J. Appl. Phys.* **98**, 124104 (2005).

- ³⁰J. Seidel, P. Maksymovych, Y. Batra, A. Katan, S.-Y. Yang, Q. He, A.P. Baddorf, S.V. Kalinin, C.-H. Yang, J.-C. Yang, Y.-H. Chu, E.K.H. Salje, H. Wormeester, M. Salmeron, and R. Ramesh, *Phys. Rev. Lett.* **105**, 197603 (2010).
- ³¹T. Ishigaki, S. Yamauchi, K. Kishio, J. Mizusaki, and K. Fueki, *J. Solid State Chem.* **73**, 179 (1988).
- ³²D.C. Arnold, K.S. Knight, F.D. Morrison, and P. Lightfoot, *Phys. Rev. Lett.*, 102, 027602 (2009).
- ³³R. Schmidt, J. Ventura, E. Langenberg, N.M. Nemes, C. Munuera, M. Varela, M.Garcia-Hernandes, C. Leon, and J. Santamaria, *Phys. Rev. B* **86**, 035113 (2012)
- ³⁴R. Schmidt, W. Eerenstein, and P.A. Midgley, *Phys. Rev. B* **79**, 214107 (2009).
- ³⁵G. Catalan, *Appl. Phys. Lett.* **88**, 102902 (2006).
- ³⁶G. Catalan and J.F. Scott, *Nature* **448**, E4 (2007).
- ³⁷J. Hemberger, P. Lunkenheimer, R. Ficht, H.-A. Krug von Nidda, V. Tsurkan, and A. Loidl, *Nature* **434**, 364 (2005).